Electronic Supplementary Material (ESI) for Physical Chemistry Chemical Physics.

Supporting Information

Mechanistic insights into the mitigation of Aβ aggregation and protofibril destabilization by a D–enantiomeric decapeptide rk10

Kamaljot Singh,[a] Anupamjeet Kaur,[a] Deepti Goyal*[b] and Bhupesh Goyal*[c]

[a] Department of Chemistry, Faculty of Basic and Applied Sciences, Sri Guru Granth Sahib World University, Fatehgarh Sahib–140406, Punjab, India

[b] Department of Chemistry, DAV College, Sector 10, Chandigarh-160011, India

[c] School of Chemistry & Biochemistry, Thapar Institute of Engineering & Technology, Patiala–147004, Punjab, India

*Corresponding author

E–mail address: deeptig@iitbombay.org; bhupesh@iitbombay.org

Table of contents

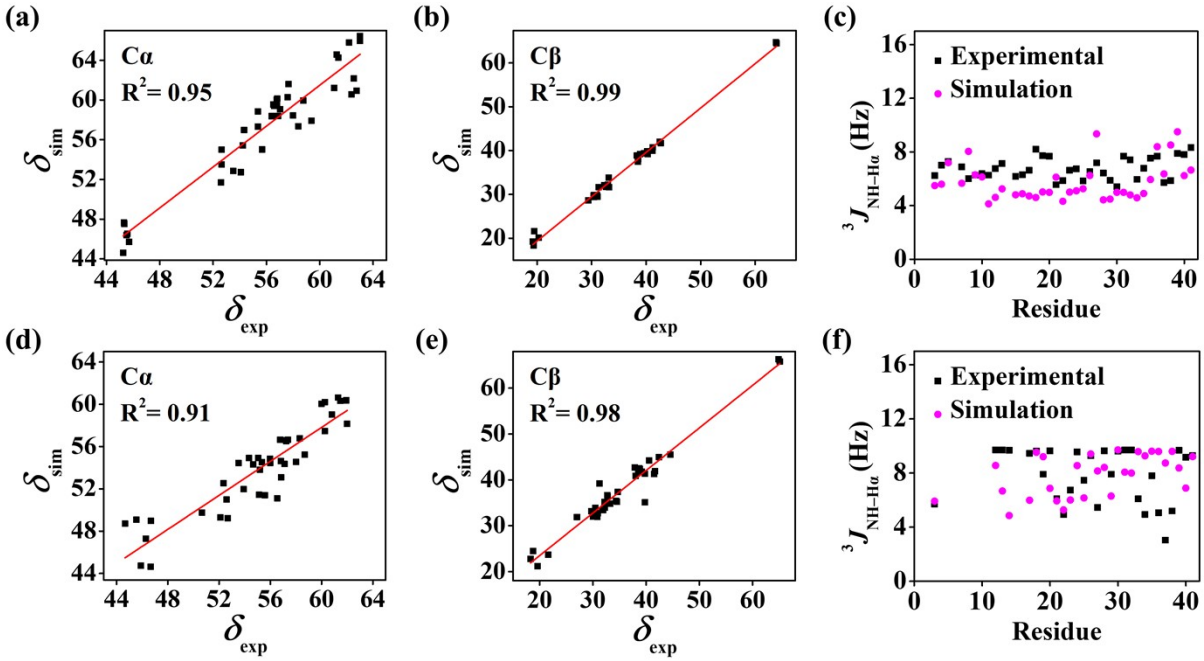

Figure S1: Comparison of NMR data obtained from simulation (δ_{sim}) with experimental (δ_{exp}) for (a) Cα chemical shift, (b) Cβ chemical shift, (c) $^{3}J_{NH–H\alpha}$ coupling constants of $A\beta_{42}$ monomer, and (d) Cα chemical shift, (e) Cβ chemical shift, (f) $^{3}J_{NH–H\alpha}$ coupling constants of $A\beta_{42}$ protofibril.

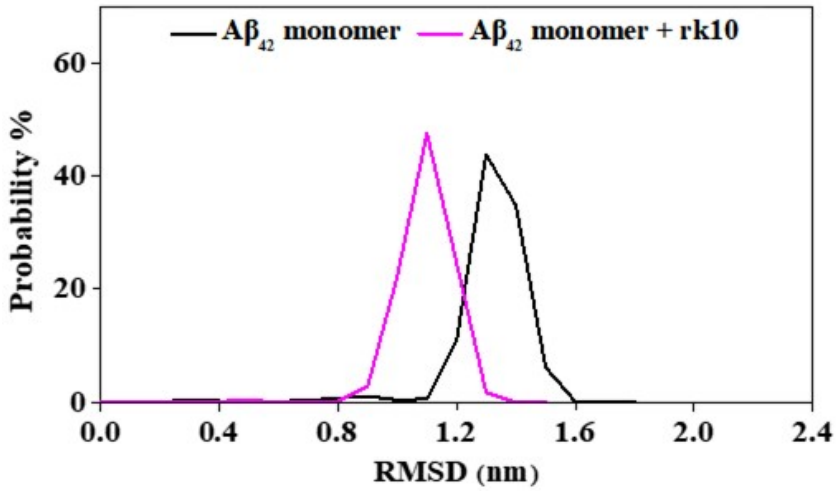

Figure S2: The probability distribution graph of RMSD for $A\beta_{42}$ monomer and $A\beta_{42}$ monomer + rk10 complex.

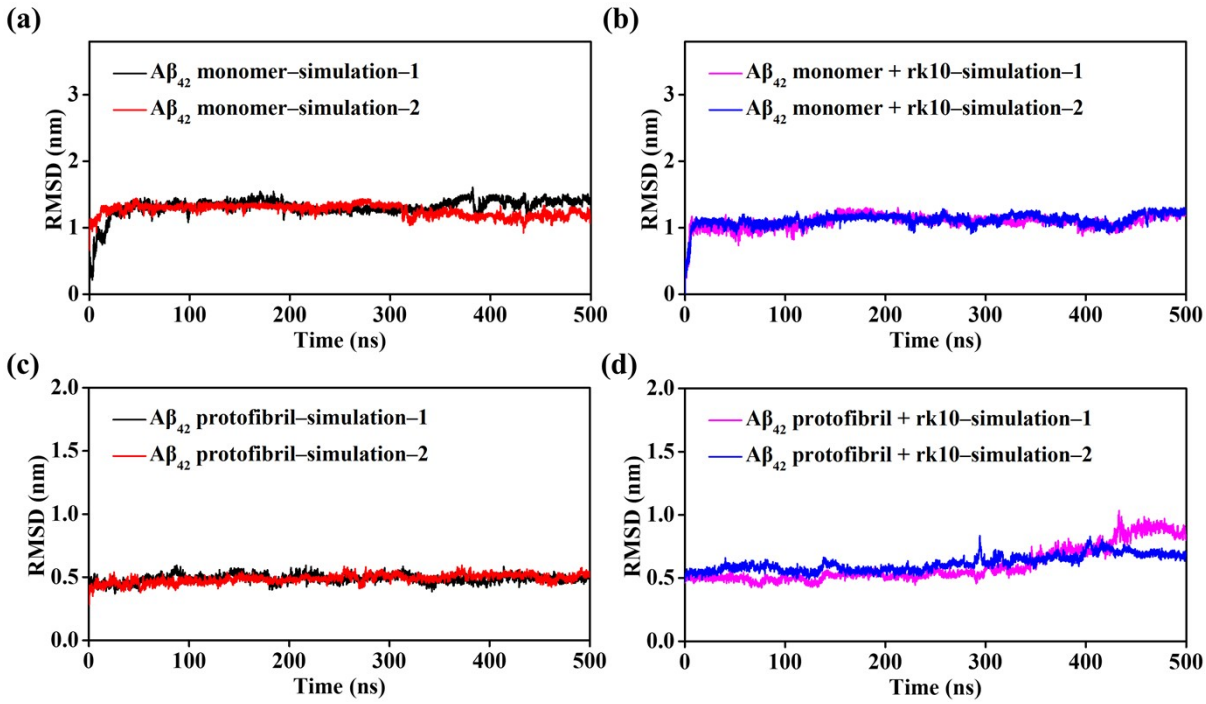

Figure S3: The RMSD of dual simulations for $A\beta_{42}$ monomer, $A\beta_{42}$ monomer + rk10 complex, $A\beta_{42}$ protofibril, and $A\beta_{42}$ protofibril + rk10 complex are shown in panel a, b, c, and d, respectively.

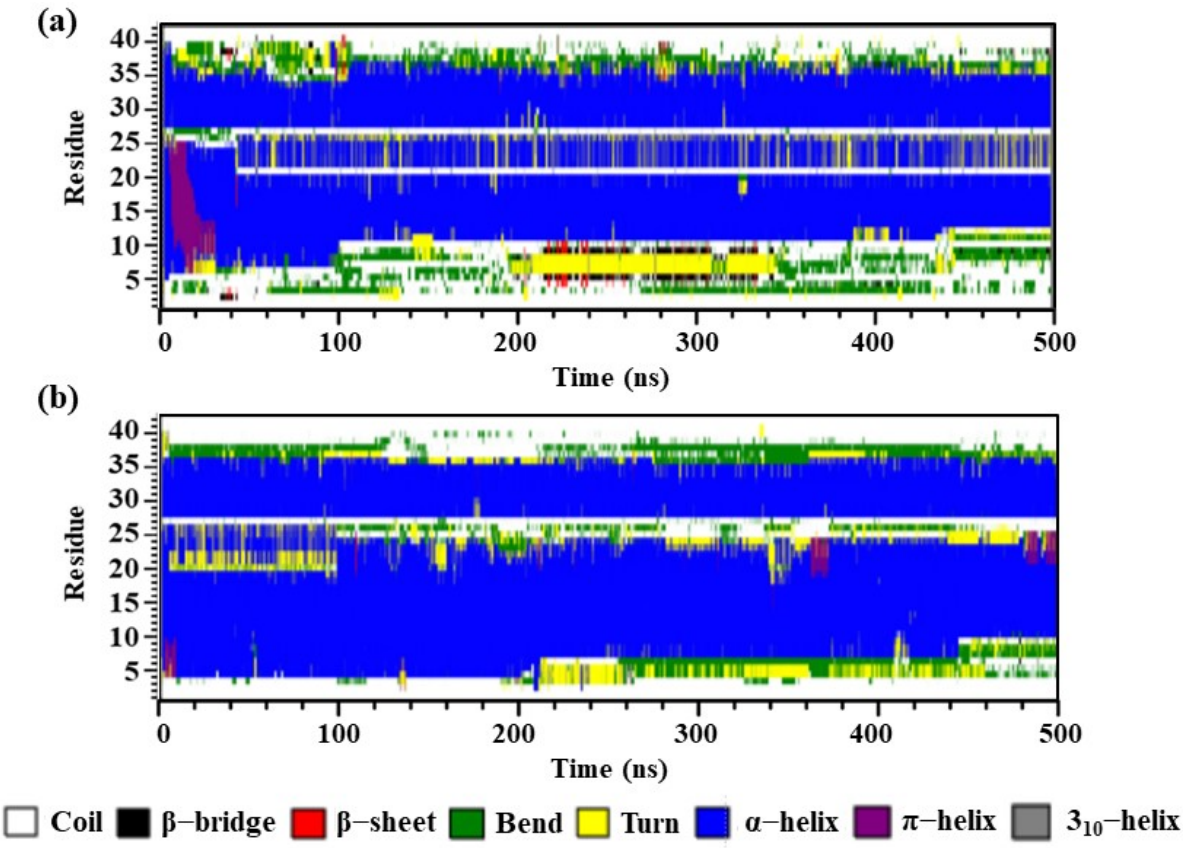

Figure S4: The evolution of secondary structure for $A\beta_{42}$ monomer (panel a) and $A\beta_{42}$ monomer + rk10 complex (panel b) during simulation. The X–axis represents simulation time in ns and Y–axis represents $A\beta_{42}$ residues. The colour-coded maps of secondary structure analysis for $A\beta_{42}$ monomer is shown underneath.

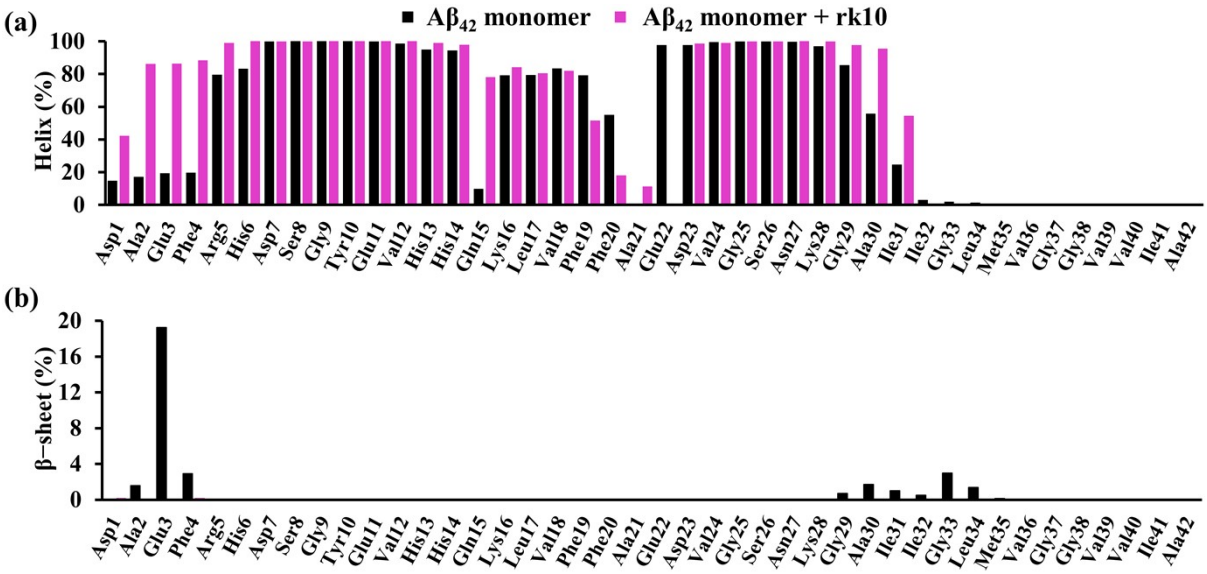

Figure S5: The per-residue helix, β–sheet percentage in $A\beta_{42}$ monomer and $A\beta_{42}$ monomer + rk10 complex are shown in panel a, and b, respectively.

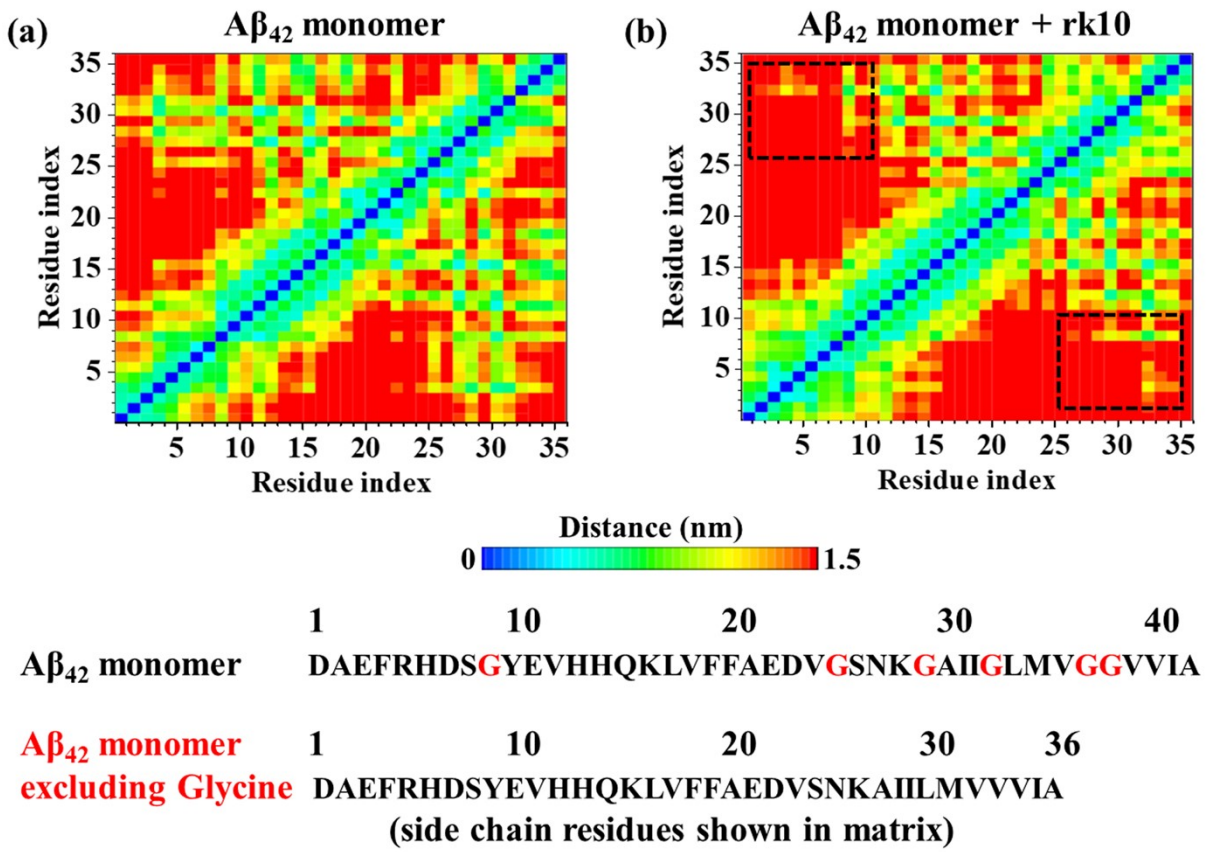

Figure S6: The side chain-side chain contact maps between $A\beta_{42}$ monomer residues in the absence and presence of rk10 are shown in panel a, and b, respectively. In the presence of rk10, the contacts between Asp1–Val12 and Ser26–Ile41 residues of $A\beta_{42}$ monomer were significantly reduced as depicted with dotted rectangular boxes in panel b.

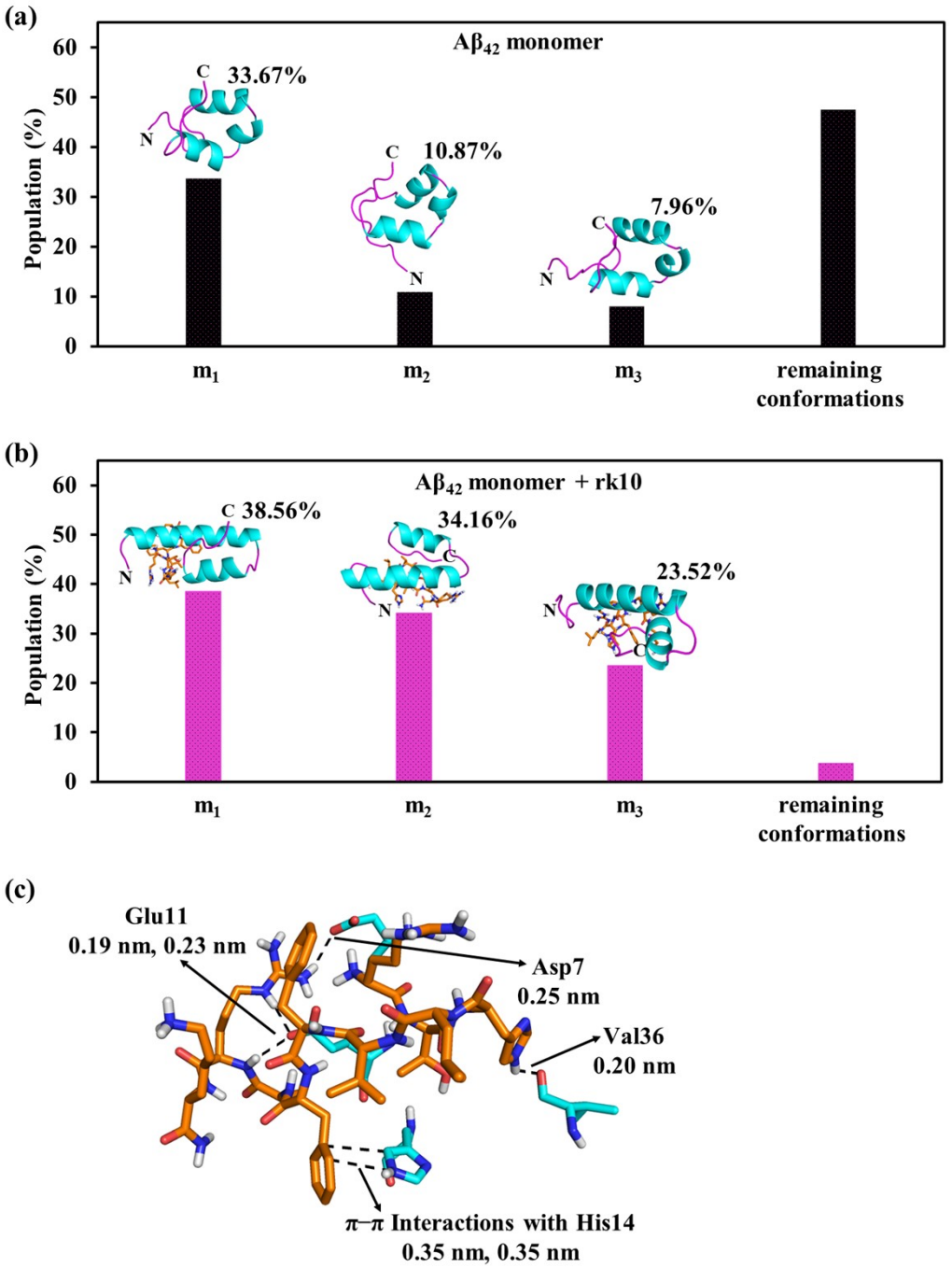

Figure S7: The representative conformations of the most-populated microstates of $A\beta_{42}$ monomer and $A\beta_{42}$ monomer + rk10 complex are shown in the cartoon representation with percentage populations in panel a, and b, respectively. The hydrogen bond and π–π interactions between $A\beta_{42}$ monomer and rk10 in the representative conformation of the most-populated microstate (m_1) of $A\beta_{42}$ monomer + rk10 complex are shown in panel c.

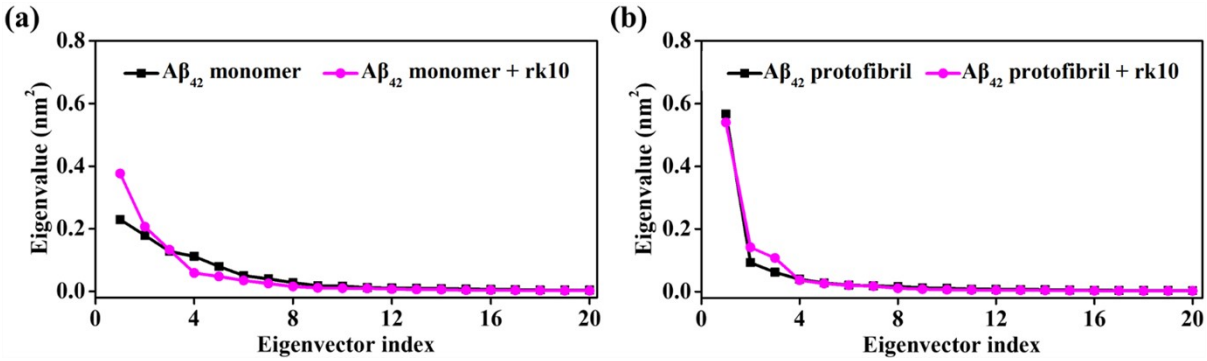

Figure S8: The eigenvalues for the corresponding eigenvectors obtained from the principal component analysis of $A\beta_{42}$ monomer (panel a) and protofibril (panel b) structures in the absence and presence of rk10.

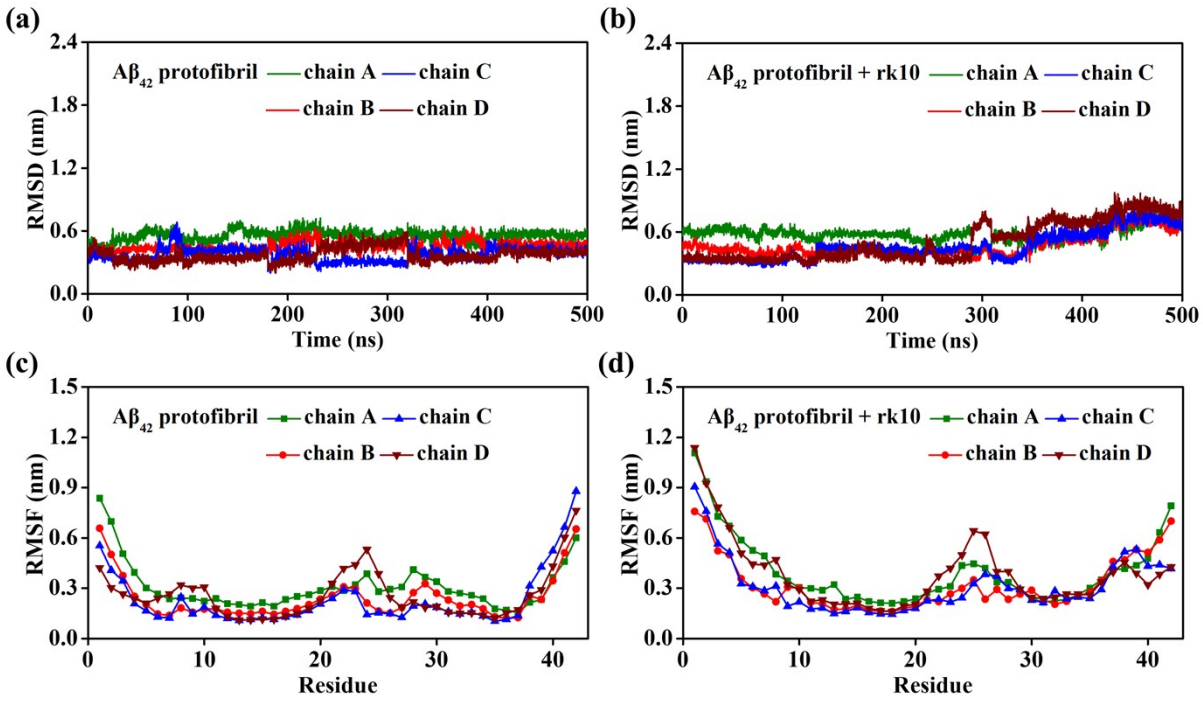

Figure S9: The RMSD for all four chains (A–D) of $A\beta_{42}$ protofibril and $A\beta_{42}$ protofibril + rk10 complex are shown in panel a, and b, respectively. The RMSF for all four chains (A–D) of $A\beta_{42}$ protofibril in the absence and presence of rk10 are shown in panel c, and d, respectively.

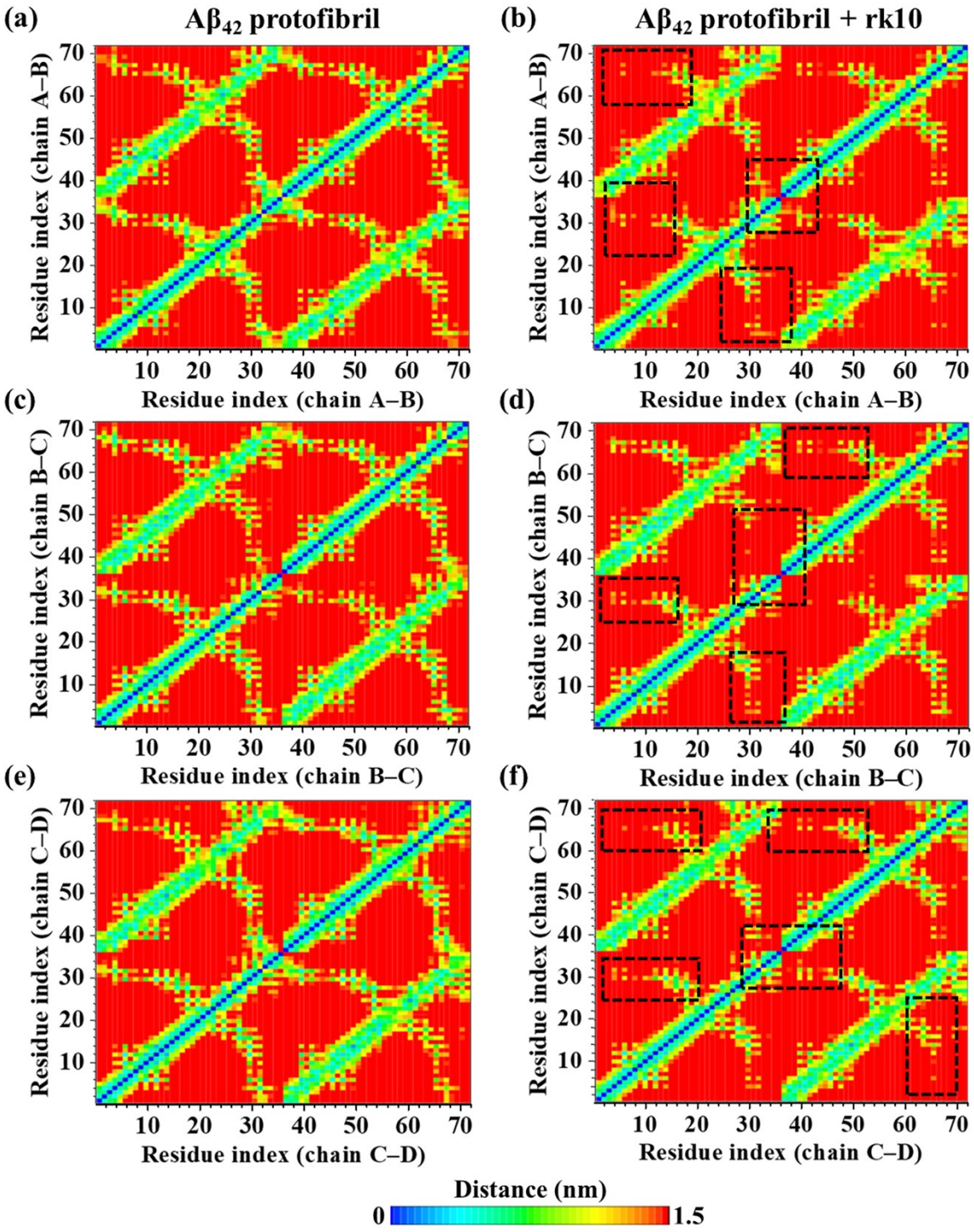

Figure S10: The side chain-side chain contact maps between $A\beta_{42}$ protofibril chains in the absence and presence of rk10. The cut-off distance between atoms used to define contact is 1.5 nm. In the presence of rk10, the strong tertiary contacts between $A\beta_{42}$ protofibril residues were disrupted as depicted with dotted rectangular boxes.

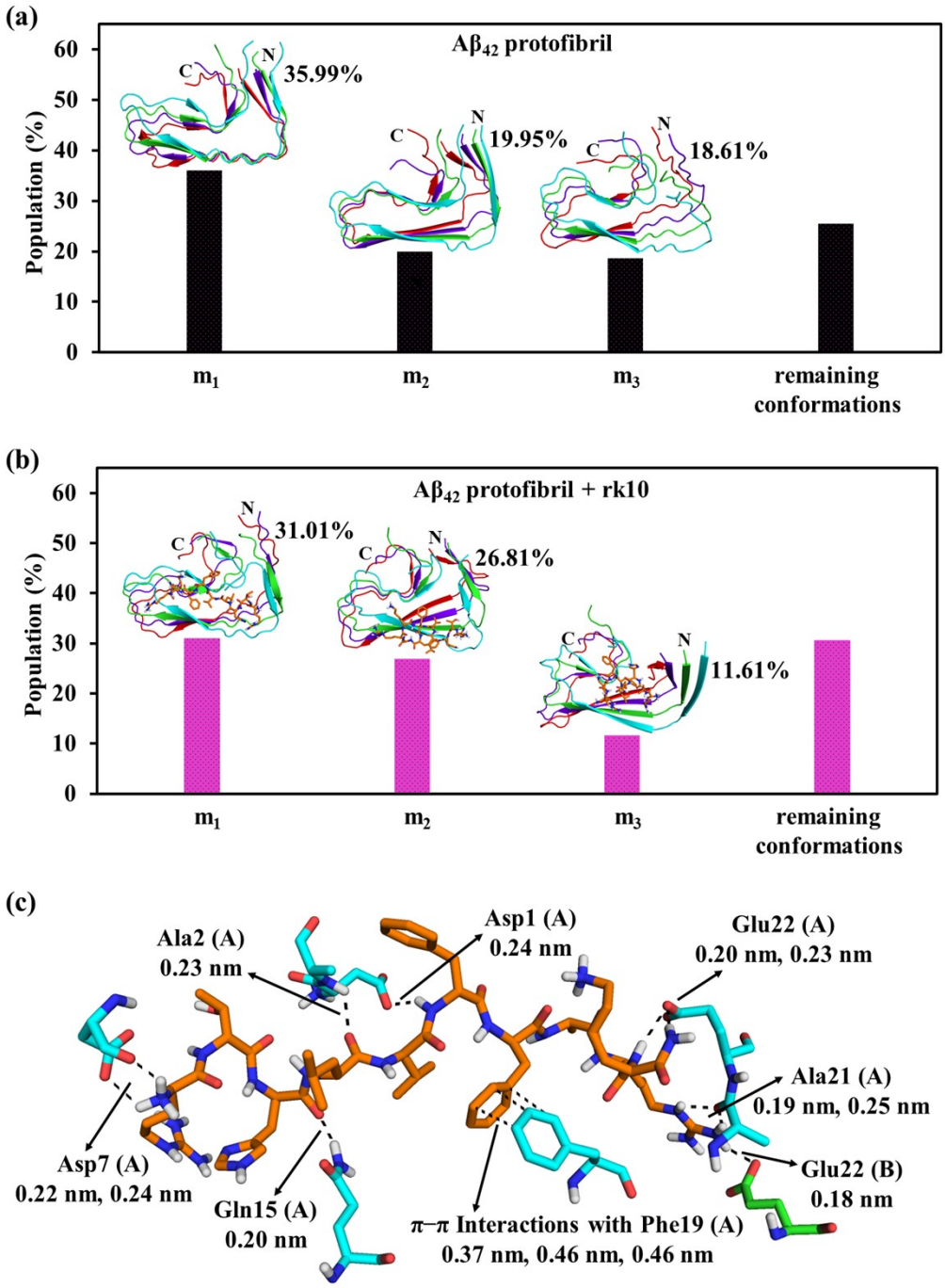

Figure S11: The representative conformations of the most-populated microstates of the $A\beta_{42}$ protofibril and $A\beta_{42}$ protofibril + rk10 complex are shown in the cartoon representation with percentage populations in panel a, and b, respectively. The hydrogen bond and π–π interactions observed in representative conformation extracted from the most-populated microstate (m_1) of $A\beta_{42}$ protofibril + rk10 complex are shown in panel c. The residues of chain A and chain B of $A\beta_{42}$ protofibril participating in hydrogen bond and π–π interactions are shown in cyan and green, respectively.

Table S1: Molecular docking analysis of rk10 with $A\beta_{42}$ monomer.

Peptide	Protein structure[a]	AutoDock binding energy (kcal/mol)	$A\beta_{42}$ residues involved in the intermolecular H–bonding interactions			$A\beta_{42}$ residues involved in intermolecular hydrophobic contacts
			Residue	Atom[b]	Distance (nm)	
rk10	$A\beta_{42}$ monomer	–5.3	Glu3	NH: O	0.23	Glu3, His6, Asp7, Ser8, Tyr10, Glu11, Val12, His14, Gln15, Phe19
			His6	NH: O	0.24	
				NH: O	0.29	
			Glu11	OH: OE1	0.19	
				NH: OE1	0.23	
				NH: OE2	0.22	
			Gln15	NH: OE1	0.23	
				CO: 1HE2	0.23	
				CO: 1HE2	0.25	
				CO: 2HE2	0.25	

[a]The PDB ID for $A\beta_{42}$ monomer used in the present study is 1IYT. [b]The atoms on left represent ligand atoms and on the right represent $A\beta_{42}$ residue atoms.

Table S2: Molecular docking analysis of rk10 with $A\beta_{42}$ monomer and protofibril structures using AutoDock Vina, Glide, and MVD.

	AutoDock Vina	Glide	MVD
$A\beta_{42}$ monomer + rk10 complex			
Binding energy (kcal/mol)	–5.3	–5.0	–15.3
Hydrogen bonds	Glu3, His6, Glu11, Gln15	Glu11, Gln15	Glu3, His6, Asp7, Gln15
Hydrophobic contacts	Glu3, His6, Asp7, Ser8, Tyr10, Glu11, Val12, His14, Gln15, Phe19	Asp7, Val12, His14, Lys16, Phe19, Phe20, Asp23	Glu3, Phe4, His6, Asp7, Tyr10, Glu11, Val12, Gln15, Phe19, Phe20
$A\beta_{42}$ protofibril + rk10 complex			
Binding energy (kcal/mol)	–6.9	–7.4	–30.3
Hydrogen bonds	Val18 (A), Phe20 (A), Glu22 (A), Ala30 (A)	Val18 (A), Phe20 (A), Glu22 (A), Ala30 (A), Ile32 (A)	Phe20 (A), Glu22 (A), Asp23 (A), Ala30 (A),
Hydrophobic contacts	Lys16 (A), Leu17 (A), Val18 (A), Phe19 (A), Phe20 (A), Ala21 (A), Glu22 (A), Asp23 (A), Val24 (A), Asn27 (A), Lys28 (A), Ala30 (A), Ile31 (A), Ile32 (A)	Leu17 (A), Val18 (A), Phe19 (A), Ala21 (A), Asp23 (A), Asn27 (A), Gly29 (A), Ile31 (A), Val40 (A), Ala42 (A)	Phe19 (A), Phe20 (A), Glu22 (A), Asp23 (A), Asn27 (A), Lys28 (A), Gly29 (A), Ala30 (A), Ile31 (A), Ala42 (A)

Table S3: The secondary structure component statistics of dual simulation for $A\beta_{42}$ monomer and $A\beta_{42}$ monomer with rk10.

System	Simulation	Secondary structure component %				
		Helix[a]	β–sheet[b]	Coil	Bend	Turn
$A\beta_{42}$ monomer	1	54.6 ± 1.59	1.2 ± 0.66	27 ± 1.52	9 ± 0.75	8.2 ± 0.71
	2	50.4 ± 4.07	2.2 ± 0.44	28.2 ± 1.66	13 ± 2.38	6.2 ± 0.52
$A\beta_{42}$ monomer + rk10	1	62.6 ±1.46	0 ± 0	22.4 ± 0.88	8.2 ± 1.24	6.8 ± 0.44
	2	58.6 ± 2.43	0.2 ± 0.18	22.6 ± 1.59	9.2 ± 1.48	9.4 ± 1.08

[a]Helix= α–helix + π–helix + 3_{10}–helix; [b]β–sheet= β–strand + β–bridge

Table S4: Molecular docking analysis of rk10 with $A\beta_{42}$ protofibril.

Peptide	Protein structure[a]	AutoDock binding energy (kcal/mol)	$A\beta_{42}$ residues involved in intermolecular hydrogen bonding			$A\beta_{42}$ residues involved in intermolecular hydrophobic contacts
			Residue	Atom[b]	Distance (nm)	
rk10	$A\beta_{42}$ protofibril	–6.9	Val18 (A) Phe20 (A) Glu22 (A) Ala30 (A)	NH: O O: NH NH: O NH: O NH: O NH: O	0.19 0.23 0.26 0.30 0.24 0.24	Lys16 (A), Leu17 (A), Val18 (A), Phe19 (A), Phe20 (A), Ala21 (A), Glu22 (A), Asp23 (A), Val24 (A), Asn27 (A), Lys28 (A), Ala30 (A), Ile31 (A), Ile32 (A)

[a]The PDB ID for $A\beta_{42}$ protofibril used in the present study is 5OQV. [b]The atoms on left represent ligand atoms and on the right represent $A\beta_{42}$ residue atoms.

Table S5: The interchain binding free energy (in kcal/mol) of the $A\beta_{42}$ protofibril in the absence and presence of rk10. The energy values are averaged over the three pairs of neighbouring chains (*i.e.*, chain A–B, chain B–C and chain C–D).

Energy components	Binding free energy (kcal/mol)	
	$A\beta_{42}$ protofibril	$A\beta_{42}$ protofibril + rk10
ΔE_{vdW}	–154.3 ± 7.0	–141.3 ± 6.9
ΔE_{elec}	13.2 ± 0.5	–7.4 ± 5.9
$\Delta E_{MM}{}^{a}$	–141.1 ± 7.5	–148.7 ± 12.8
ΔG_{ps}	142.4 ± 25.5	155.9 ± 22.3
ΔG_{nps}	–149.6 ± 11.7	–142.3 ± 11.9
$\Delta G_{solv}{}^{b}$	–7.2 ± 13.8	13.6 ± 10.4
$\Delta G_{binding}{}^{c}$	–148.3 ± 21.3	–135.1 ± 2.4

$^{a}\Delta E_{MM} = \Delta E_{vdW} + \Delta E_{elec}$; $^{b}\Delta G_{solv} = \Delta G_{ps} + \Delta G_{nps}$; $^{c}\Delta G_{binding} = \Delta E_{MM} + \Delta G_{solv}$

Table S6: The interchain (*i.e.*, chain A–B, chain B–C and chain C–D) binding free energy (in kcal/mol) of the $A\beta_{42}$ protofibril in the absence and presence of rk10.

Systems	Chain	ΔE_{vdw}	ΔE_{elec}	ΔE_{MM}[a]	ΔG_{ps}	ΔG_{nps}	ΔG_{solv}[b]	$\Delta G_{binding}$[c]
$A\beta_{42}$ protofibril	A–B	–153.2 ± 7.4	–13.7 ± 30.2	–166.9 ± 37.6	157.7 ± 36.9	–151.8 ± 13.3	5.9 ± 23.6	–161.0 ± 14.0
	B–C	–153.2 ± 6.7	52.2 ± 18.2	–101.0 ± 11.5	123.4 ± 23.1	–145.7 ± 11.2	–22.3 ± 11.9	–123.3 ± 23.4
	C–D	–156.4 ± 7.0	1.1 ± 13.6	–155.3 ± 6.6	146.2 ± 16.6	–151.2 ± 10.7	–5.0 ± 5.9	–160.3 ± 12.5
$A\beta_{42}$ protofibril + rk10	A–B	–127.9 ± 7.1	–30.7 ± 18.4	–158.6 ± 25.5	176.3 ± 21.0	–134.9 ± 12.9	41.4 ± 8.1	–117.2 ± 17.4
	B–C	–143.4 ± 6.9	6.9 ± 16.6	–136.5 ± 9.7	136.3 ± 23.6	–142.8 ± 11.6	–6.5 ± 12.0	–143.0 ± 21.7
	C–D	–152.7 ± 6.7	1.6 ± 19.4	–151.1 ± 12.7	155.2 ± 22.3	–149.1 ± 11.2	6.1 ± 11.1	–145.0 ± 1.6

[a]$\Delta E_{MM} = \Delta E_{vdw} + \Delta E_{elec}$; [b]$\Delta G_{solv} = \Delta G_{ps} + \Delta G_{nps}$; [c]$\Delta G_{binding} = \Delta E_{MM} + \Delta G_{solv}$